JCI insight

Noise induces Ca2+ signaling waves and Chop/S-Xbp1 expression in the hearing cochlea

Yesai Park, … , Elliott H. Sherr, Dylan K Chan

JCI Insight. 2024. https://doi.org/10.1172/jci.insight.181783.

Research In-Press Preview Otology

Graphical abstract

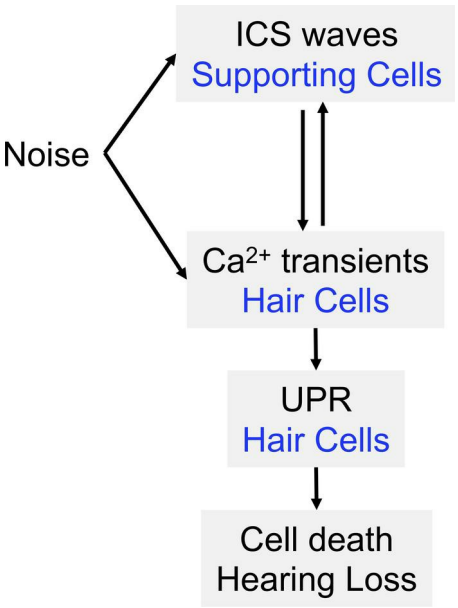

Title: Noise induces Ca^{2+} signaling waves and *Chop*/*S-Xbp1* expression in the hearing cochlea

Authors:

*Yesai Park[1], *Jiang Li[2,3], Noura Ismail Mohamad[1], Ian R. Matthews[1], Peu Santra[1], †Elliott H. Sherr[2,3], and †Dylan K. Chan[1]

Affiliations:

1. Department of Otolaryngology-Head and Neck Surgery, UCSF
2. Department of Neurology, University of California, San Francisco (UCSF)
3. Department of Pediatrics, Institute of Human Genetics, Weill Institute for Neurosciences, UCSF

*These authors share first position.

†These authors share final position. Correspondence should be addressed to them as follows:

Dylan K. Chan, MD, PhD

Department of Otolaryngology-Head and Neck Surgery, UCSF

513 Parnassus Ave, Rm 719

San Francisco, CA 94143

dylan.chan@ucsf.edu

415-353-2757

and

Elliott H. Sherr MD, PhD

Department of Neurology, Institute of Human Genetics
675 Nelson Rising Lane, Room 214B
San Francisco, CA 94158
Elliott.sherr@ucsf.edu
415-502-8039

Conflict of Interest Statement: EHS and DKC are co-owners of Jacaranda Biosciences, Inc . EHS is co-inventor on a US provisional patent application: “Novel Methods of Treating Hearing Loss” (PCT/US2016/058348). None of the authors have financial relationships with the organizations that sponsored the research.

Abstract

Exposure to loud noise is a common cause of acquired hearing loss. Disruption of subcellular calcium homeostasis and downstream stress pathways in the endoplasmic reticulum and mitochondria, including the unfolded protein response, have been implicated in the pathophysiology of noise-induced hearing loss. However, studies on the association between calcium homeostasis and stress pathways have been limited due to limited ability to measure calcium dynamics in mature-hearing, noise-exposed mice. We used a genetically encoded calcium indicator mouse model in which GCaMP is expressed specifically in hair cells or supporting cells under control of Myo15Cre or Sox2Cre, respectively. We performed live calcium imaging and UPR gene expression analysis in 8-week-old mice exposed to levels of noise that cause cochlear synaptopathy (98 db SPL) or permanent hearing loss (106 dB SPL). UPR activation occurred immediately after noise exposure and was noise dose-dependent, with the pro-apoptotic pathway upregulated only after 106 dB noise exposure. Spontaneous calcium transients in hair cells and intercellular calcium waves in supporting cells, which are present in neonatal cochleae, were quiescent in mature-hearing cochleae, but re-activated upon noise exposure. 106 dB noise exposure was associated with more persistent and expansive intercellular Ca^{2+} signaling wave activity. These findings demonstrated a strong and dose-dependent association between noise exposure, UPR activation, and changes in calcium homeostasis in hair cells and supporting cells, suggesting that targeting these pathways may be effective to develop treatments for noise-induced hearing loss.

Introduction

Noise-induced hearing loss (NIHL) affects an estimated 40 million individuals in the US, with no approved medical treatments (1). A number of cellular mechanisms have been proposed to be involved in NIHL, including oxidative stress (2,3), JNK/ERK pathway activation (4), mitochondrial stress (5), endoplasmic reticulum (ER) stress, and the Unfolded Protein Response (UPR) (6); targeting these pathways have identified multiple candidate drugs that prevent NIHL to varying degrees in mouse: Ru360, a mitochondrial Ca^{2+} uniporter (MCU) inhibitor that reduces mitochondrial Ca^{2+} uptake and overload (7); ISRIB, an eIF2B activator that inhibits the pro-apoptotic PERK/CHOP pathway of the UPR (6); D-JNKI-1, a peptide inhibitor of c-Jun N-Terminal Kinase that blocks the MAPK-JNK signaling pathway (8); and N-acetyl cysteine, an antioxidant that reduces reactive oxygen species and oxidative stress (9). Of these, D-JNKI-1 and NAC have been tested in humans and shown limited efficacy in reducing NIHL (10,11). Better understanding of the precise mechanistic pathways by which noise induces cellular pathways in the cochlea leading to sensory hair-cell death is essential to develop more effective treatments.

Many of these potential pathways – mitochondrial/oxidative stress, and ER stress and the UPR — are activated upon disruption of Ca^{2+} homeostasis. In addition to acquired hearing loss, many genetic forms of deafness involve molecules involved in Ca^{2+} flow and homeostasis in cochlear cells (12), illustrating the broad-based importance of these pathophysiologic mechanisms. Dysregulation of subcompartmental Ca^{2+} homeostasis has been directly implicated in hair cell death using an aminoglycoside model of ototoxicity in zebrafish hair cells, in which ER Ca^{2+} depletion leads to cytosolic Ca^{2+} accumulation, mitochondrial Ca^{2+} overload, and mitochondrial stress (13,14). In mammals, both ER Ca^{2+} depletion (leading to UPR activation) and mitochondrial Ca^{2+} overload (leading to oxidative stress) have been implicated in hearing loss (6, 8). We have shown that disruption of TMTC4, an ER-resident, hair cell-specific gene implicated in progressive hearing loss in mice and humans (15), causes ER Ca^{2+} depletion

and UPR activation, and that noise exposure causes UPR activation (6). Importantly, we found that targeting the UPR with ISRIB, a small molecule activator of eIF2B, reduces noise-induced hearing loss and cochlear synaptopathy (6,16). On the other hand, genetic or pharmacologic disruption of MCU, which reduces mitochondrial Ca^{2+} accumulation, also protects against NIHL (7). Despite this strong evidence that disruption of Ca^{2+} homeostasis in hair cells can lead to hair cell death through ER- and/or mitochondrial stress pathways, it is not clear how, and whether, noise trauma directly causes this Ca^{2+} dysregulation in hair cells.

One possibility is that mechanical trauma or noise exposure affects Ca^{2+} homeostasis through induction of intercellular Ca^{2+} signaling (ICS) waves in supporting cells. ICS waves have been studied extensively in the central nervous system; they propagate across glial networks, where they respond to mechanical and excitotoxic trauma and mediate neuronal repair, death, and migration (17,18). Noise and mechanical trauma have also been suggested to induce ICS waves across supporting cell networks in the cochlea (19), but not hair cells; ICS waves are dependent on Cx26 to propagate, and Cx26 is only expressed in supporting cells (20). These changes in Ca^{2+} flux have been implicated in downstream cellular signaling cascades, including activation of the ERK pathway (21) as well as the UPR (6). In the neonatal cochlea, ICS waves occur spontaneously in supporting cells of the inner sulcus (IS) and outer sulcus (OS) in the late stages of cochlear development, synchronizing inner-hair-cell (IHC) firing (22,23). ICS waves can also be triggered in neonatal cochleae by external ATP or direct mechanical trauma (19,26). Though spontaneous ICS activity was initially thought to become quiescent after the onset of hearing (23), subsequent studies have shown limited evidence of spontaneous (24) and noise-evoked (16) ICS waves in the adult mouse and gerbil cochlea, respectively. The role of these supporting cell ICS waves in the inner ear's response to noise, however, is poorly understood.

Despite these studies demonstrating links between noise exposure and ICS signaling in supporting cells in mechanically traumatized neonatal cochlea (19), between Ca^{2+} transients in hair cells and cell death in zebrafish aminoglycoside ototoxicity (13,14), and between ER and

mitochondrial stress and noise exposure in mice (6,7), comprehensive evaluation of the Ca^{2+} and stress pathways by which noise exposure leads to hearing loss has been limited due to the absence of a single experimental model in which dynamic cellular processes can be observed live in the mature, hearing cochlea after physiologically relevant noise exposure. Such work would require a single model system in which the effect of noise exposures on Ca^{2+} homeostasis in hair cells and supporting cells can be directly correlated with the effect of the same noise exposures on downstream pre-apoptotic pathways, such as the UPR, and hearing loss.

In this study, we sought to evaluate the hypothesis that excessive noise induces Ca^{2+} homeostatic changes in both hair cells and supporting cells, leading ultimately to pro-apoptotic UPR activation. In order to do this, we have developed a live-imaging model of the mature, hearing cochlea, enabling direct visualization of cytosolic Ca^{2+} dynamics in hair cells and supporting cells after physiologically-relevant noise exposure. This model allows us to measure three elements of the Ca^{2+} dysregulation/UPR axis in response to the same set of physiologically-relevant noise exposures that cause either temporary or permanent shifts in hearing thresholds: 1) UPR gene expression; 2) Ca^{2+} transients in hair cells; and 3) ICS waves in supporting cells. Evidence of these three phenomena provides support that they are all connected in the early response of the cochlea to acoustic overstimulation.

Results

UPR expression after NIHL

We first investigated the response of the UPR to varying levels of noise exposure. 8-week-old male and female wild-type CBA/J mice were exposed to 8-16 kHz octave-band noise for 2h at three levels: 94 dB SPL, which does not cause any threshold shift; 98 dB SPL, which causes

temporary threshold shift (TTS) and cochlear synaptopathy (16); and 106 dB SPL, which causes permanent threshold shift (PTS) and hair cell death (6) (**Supplemental Figure S1, S2**). Cochleae were extracted from mice 2 hours after completion of noise exposure, and expression levels of three UPR marker genes – *BiP*, *Chop*, and *S-Xbp1* – were measured by qPCR (**Figure 1**). *BiP*, a marker for general activation of the UPR, was significantly elevated with all noise exposure levels, demonstrating that noise exposure upregulates the UPR. No significant changes in *S-XBP1*, a specific marker for the pro-homeostatic arm of the UPR, were seen compared to control. *Chop*, a marker of the pro-apoptotic arm of the UPR, was elevated only in male mice exposed to 106 dB SPL. However, when the ratio of *Chop*/*S-Xbp1*, which indicates a shift in the balance of the UPR towards apoptosis (27,28), was compared across conditions, significant elevation of this ratio was seen in both male and female mice exposed to 106 dB SPL noise. These results demonstrate that although the UPR is activated overall with any noise exposure (as indicated by *BiP*), noise levels that cause PTS and hair cell loss are associated specifically with significant elevation of the *Chop*/*S-Xbp1* ratio. Overall, no statistically significant differences were seen relating to biological sex; for this reason, all subsequent experiments were pooled across sexes.

In addition to qPCR for UPR marker genes, we measured the expression of 84 UPR genes using an mRNA expression panel after 106 dB SPL noise exposure compared with unexposed controls. This showed that *Ddit3* (*Chop*) (1.92x, $p = 0.006$) and as well as *Hspa5* (*BiP*; 2.21x, $p=0.01$) were statistically significantly upregulated in mice exposed to 106 dB SPL noise, consistent with single-gene qPCR findings (**Figure 1**). Among other genes on the panel, *Cepbp* (5.51x, $p < 0.0001$), which was previously implicated as an overexpressed gene in the proteotoxic stress response during NIHL (29), was most markedly upregulated. The findings from this panel were from bulk cochleae, but are consistent with analysis of hair cell-specific data from prior RNASeq experiments obtained from mice exposed to 105 dB SPL noise, very similar to the 106 dB SPL noise-exposure protocol used in the current study (30; umgear.org).

These data showed that in purified outer hair cells (OHCs), both *Ddit3* (1.58x overexpression, p = 0.0077) and *Cebpb* (3.24x, p = 0.00016) were very significantly upregulated by noise (**Supplemental Figure S3A,** top). In contrast, purified SCs from the same dataset showed statistically significant noise-induced upregulation of *Cebpb* (2.98x, p = 0.005), but not *Ddit3* (1.32x, p = 0.15; **Supplemental Figure S3A,** bottom). Finally, upregulation of *Ddit3*/*Chop* in specific cell types within the cochlea was examined by whole-mount immunohistochemistry, which showed that 106 dB SPL noise caused upregulation of *Chop* in OHCs, IHCs, and inner pillar cells (**Supplemental Figure S3B**).

We next investigated the time-course of UPR activation after 98 and 106 dB SPL noise exposure, our two primary models for TTS and PTS, respectively. Cochleae were harvested at 0, 2, 12, and 24h after completion of the 2h noise exposure, as well as 2 weeks later, and compared with control, non-noise-exposed animals (**Figure 2**). Elevation in *BiP* was seen immediately after noise exposure, followed by changes in *Chop* and *S-Xbp1*. Elevation in *Chop*/*S-Xbp1* ratio peaked at 2h after noise exposure and was more pronounced in mice exposed to the louder 106 dB SPL noise. These findings demonstrate that UPR gene expression changes are an early and dose-dependent response to noise exposure in mice.

Live Ca^{2+} imaging in hair cells and supporting cells in the neonatal cochlea

We then sought to use these same noise-exposure models —98-dB and 106-dB, 8-16 kHz octave-band noise, which are associated with TTS (and UPR activation without shift towards apoptosis) and PTS (with pro-apoptotic UPR activation), respectively — and directly visualize Ca^{2+} dynamics in the organ of Corti. However, live Ca^{2+} imaging had previously been performed primarily in neonatal cochlear cultures, which cannot be stimulated with sound, and prior instances of Ca^{2+} imaging in the adult cochlea (24,26) used exogenous dyes that did not sufficiently label hair cells. We therefore developed an acute explant preparation of the temporal

191 bone from juvenile, mature-hearing mice (31) expressing the cytosolic Ca^{2+} indicator GCaMP6f
192 in a Cre-dependent manner in supporting cells (driven by Sox2Cre) or hair cells (driven by
193 Myo15Cre). This preparation was similar to one previously described that demonstrated ICS
194 waves in the adult mouse using exogenous Fluo-4-AM dye for Ca^{2+} sensing (24), but instead
195 uses a genetically-encoded Ca^{2+} indicator to further expedite imaging after euthanasia and
196 enable both hair cell- and supporting cell-specific labeling.
197 To validate this model, we first confirmed expression of GCaMP and validated its ability
198 to detect Ca^{2+} activity in supporting cells and hair cells in neonatal mice. Neonatal cochlear
199 cultures from Sox2Cre-GCaMP mice expressed GCaMP in supporting cells, but not hair cells
200 (**Figure 3**), and exhibited spontaneous ICS waves identical to those seen using exogenous
201 fluorophores (FURA-2 (19) and Fluo-4 (22,24)). ICS waves were observed in Kölliker's organ at
202 the IS, as well as in OS (**Supplemental Video 1, Figure 3**). Overall, ICS waves propagated at
203 15.5 ± 0.5 μm/s (mean ± sem from 128 waves in 15 cochleae) in the IS and 27.9 ± 0.4 μm/s
204 (N=914 waves) in the OS, and occurred at a rate of 0.03 waves/s (IS) and 0.20 waves/s (OS).
205 Drugs that prevent cytosolic Ca^{2+} clearance —vanadate, which blocks extrusion through PMCA,
206 and thapsigargin, which blocks ER re-uptake through SERCA — affected both single-cell-level
207 Ca^{2+} peaks and ICS characteristics. 5 μM vanadate, but not 1 μM thapsigargin, increased the
208 frequency of Ca^{2+} peaks and ICS waves (**Figure 3B,F**). Both drugs significantly increased the
209 decay time for the cytosolic Ca^{2+} peak to return back to baseline (**Figure 3C-E**); thapsigargin,
210 but not vanadate, increase the distance of ICS wave propagation (**Figure 3G-H**). Finally,
211 vanadate, but not thapsigargin, increased steady-state cytosolic Ca^{2+} levels (**Figure 3I-J**). In
212 contrast to these effects of vanadate and thapsigargin, tunicamycin, which induces ER stress
213 but does not directly impact ER Ca^{2+} dynamics, had no effect on Ca^{2+} activity in neonatal
214 cochleae other than a small increase in decay time (**Supplemental Figure S4**). Taken

together, these findings suggest that supporting-cell-specific GCaMP signal in the Sox2Cre-GCaMP model is accurately representing ICS wave activity.

We then examined neonatal cultures from Myo15Cre-GCaMP mice, which express GCaMP in hair cells with scant off-target labelling (**Supplemental Video 2**, **Figure 4).** Minimal spontaneous activity was observed (**Supplemental Video 2**); occasional spontaneous Ca^{2+} transients were observed in IHCs, but these never propagated as ICS waves, consistent with the fact that hair cells do not express connexin 26 necessary for the direct and paracrine signaling that underlies wave propagation (20). Application of ATP, however, induced a large cytosolic Ca^{2+} transient in both IHCs and OHCs, demonstrating intact purinergic responses; clearance of these ATP-induced Ca^{2+} peaks was sensitive to vanadate and thapsigargin in IHCs, but not OHCs (**Figure 4B-C**). Application of TG and VN induced initial increases in Ca^{2+} in both IHCs and OHCs (**Figure 4D-E**); however, steady-state Ca^{2+} was only significantly raised by TG in OHCs, whereas VN increased steady-state Ca^{2+} in both types of hair cells (**Figure 4F-G**) illustrating distinct patterns of Ca^{2+} homeostasis in IHCs and OHCs.

Live Ca^{2+} imaging in hair cells and supporting cells in the mature, hearing cochlea

Having established the ability to perform hair-cell and supporting-cell-specific live cytosolic Ca^{2+} imaging in neonatal cochlea, we moved to our juvenile (7-8-week-old), mature-hearing cochlear preparation, which enables imaging of the 8-10 kHz region of the cochlea (31,32). GCaMP-expressing mice have similar baseline hearing thresholds and response to 98-dB and 106-dB SPL noise exposures as wild-type CBA/J mice (**Supplemental Figure S5**). GCaMP expression was visible in both hair cells (in Myo15Cre-GCaMP mice) and supporting cells (in Sox2Cre-GCaMP mice), and cells remained stable in shape and size, with no steady-state changes in cytosolic Ca^{2+} levels over the recording period, suggestive of overall cellular health in this explant preparation (**Supplemental Videos 3-4**). There were no spontaneous intracellular Ca^{2+}

transients seen in hair cells (**Supplemental Video 3**). In supporting cells, which exhibited robust spontaneous activity in both IS and OS regions of the neonatal cochlea, reduced spontaneous activity was observed in these regions of the mature-hearing cochlea, though some activity was seen in Deiters' cells (**Supplemental Video 4, Figure 5**). This is consistent with prior report, which demonstrated quiescence of spontaneous ICS wave activity after the onset of hearing around postnatal day 14 (23). Overall, these findings demonstrate that the mature-hearing cochlear explant preparation from Myo15Cre-GCaMP and Sox2Cre-GCaMP is healthy and enables detection of cytosolic Ca^{2+}, but that overall Ca^{2+} activity is quiescent under control, non-noise-exposed conditions.

Noise exposure activates ICS activity in cochlear supporting cells

Though spontaneous ICS waves in supporting cells of the mature-hearing cochlea were scant, noise exposure elicited increased ICS activity (**Supplemental Video 5, Figure 6A**). ICS waves propagated across and between all supporting-cell types: phalangeal, inner and outer pillar, Deiters', and Hensen's cells. 8-16 kHz octave-band noise at 98 and 106 dB SPL, which elicits TTS with cochlear synaptopathy and PTS with hair-cell death, respectively, both induced a significant increase in the number of cell-level Ca^{2+} transients as well as organ-level ICS waves within 1h of initiation of noise (peaks/s (mean ± sem): 98 dB, 1.90 ± 0.16; 106 dB, 1.62 ± 0.39; unexposed, 0.75 ± 0.15; $p = 0.0036$, one-way ANOVA; waves/s: 98 dB, 0.20 ± 0.03; 106 dB, 0.11 ± 0.02; unexposed, 0.07 ± 0.02; $p = 0.0046$, one-way ANOVA; **Figure 6B-C**). 24h after completion of a full 2h noise exposure, cochleae exposed to 106 dB SPL noise, which ultimately causes hair-cell death, had persistent Ca^{2+} peak activity (1.62 ± 0.39 peaks/s, 0.25 ± 0.05 waves/s), whereas those exposed to 98 dB SPL noise did not (1.28 ± 0.26 peaks/s, 0.12 ± 0.03 waves/s). For both noise exposure levels, the decay time of the Ca^{2+} transients in these supporting cells, which is a measure of persistent cytosolic Ca^{2+} elevation, was not significantly

elevated (**Figure 6D-E**). At the ICS wave level, cochleae exposed to 106 dB SPL noise had significantly longer distance of ICS wave propagation at both timepoints compared to control as well as 98-dB-exposed cochleae (**Figure 6F-G**). Taken together, these findings demonstrate that noise exposure induces ICS wave activity in cochlear supporting cells, and that this ICS-related cytosolic Ca^{2+} elevation is more persistent and extensive in cochleae exposed to the louder 106 dB SPL noise dose.

Cochlear hair cells are not responsive to noise or ATP but demonstrate cytosolic Ca^{2+}-associated cell death after noise exposure.

Adult cochlear hair cells displayed no spontaneous Ca^{2+} transients (**Supplemental Video 3**). Unlike neonatal hair cells, adult hair cells were not even responsive to external ATP. Application of 1 μM ATP elicited a robust Ca^{2+} transient in IS supporting cells with off-target expression of GCaMP, but not the adjacent hair cells (**Figure 7A-B**). 106 dB SPL noise exposure elicited Ca^{2+} transients in OHCs (**Supplemental Video 6**). These transients could be clearly differentiated into two types based on rise and decay kinetics and cross-sectional area of the associated OHCs (**Figure 7C-D**). 7/80 OHCs (8.8% of all OHCs, rate of 3.5 transients/min) exhibited "fast" transients with rapid onset and decay back to baseline, and did not show changes in hair-cell morphology (**Figure 7E**), though the decay times (27.2 ± 6.8 s (mean ± s.e.m.)) were significantly longer than those seen for Ca^{2+} transients in supporting cells (2.52 ± 0.06 s for 106-dB noise exposure, **Figure 6D,** $p < 0.0001$ compared to hair cells). 13/80 OHCs (16.3% of all OHCs, rate of 6.5 transients/min) exhibited "slow" Ca^{2+} transients that occurred over an even longer timecourse, and preceded hair-cell swelling and fragmentation consistent with cell death (**Figure 7F**).

Discussion

In this study, we used a mature-hearing, physiologically relevant model of NIHL to evaluate critical components of ER stress – activation of the UPR and alterations of Ca^{2+} homeostasis within hair cells and supporting cells – in the cochlear response to acoustic overstimulation. We found that the UPR is indeed activated immediately after multiple levels of noise exposure, peaking within 2h (**Figure 2**), with a shift towards the pro-apoptotic PERK/CHOP pathway only with the 106 dB noise exposure level that causes permanent threshold shifts and hair-cell death (**Figure 1**). Our findings corroborate and extend prior results in a physiological model of NIHL. Early upregulation of UPR genes has been suggested in cell-specific RNASeq analysis of noise-exposed mice (30), with specific genes - *Ddit3* and *Cebpb* in particular - significantly upregulated after 105 dB SPL exposure. Some inconsistencies exist, however; for example, in our prior study, 106 dB noise exposure induced upregulation of *Chop*, *BiP*, and *S-Xbp1* in FVB mice, whereas in the current study only *Chop* and *BiP* were increased in CBA/J mice, implying strain differences. The aforementioned RNASeq atlas (30) was obtained from Ai14 mice, and the Ca^{2+} imaging performed in the current study was performed in the C57/Bl6 strain, which may have other strain-specific differences in UPR responses. Furthermore, the absence of upregulation of other pro-apoptotic factors, such as *Atf4*, in both our data and previous study (30) suggests complexity in noise-induced UPR regulation that must be understood. Our evaluation of UPR upregulation was limited to selected marker genes at the mRNA expression level; we did not explore more complex gene pathway alterations or downstream proteomic and phosphorylation changes that occur as part of the UPR and downstream apoptosis, which may be pursued in future studies.

Finally, we measured UPR gene expression in both male and female mice exposed to noise. Though we did not observe any sex-based difference in *Chop*/*S-Xbp1* ratio, there was a difference in CHOP expression after 106-dB SPL noise exposure between male and female mice, though this was not statistically significant after correcting for multiple comparisons

(**Figure 1**). We have previously observed sex differences in UPR-targeted treatment of noise-induced cochlear synaptopathy (16), suggesting that there may be sex differences in the UPR response to noise that the current study is underpowered to detect.

After demonstrating that a genetically-encoded Ca^{2+} indicator model that expresses GCaMP specifically in hair cells or supporting cells accurately reports cytosolic Ca^{2+} in neonatal cochleae (**Figures 3-4**), we studied the exact same noise-exposure models in mature-hearing, 7-8-week-old mice. Whereas neonatal, developing cochlea exhibited abundant spontaneous Ca^{2+} activity, especially ICS waves in supporting cells, both hair cells and supporting cells in the mature-hearing cochlea showed minimal spontaneous cytosolic Ca^{2+} transients or ICS waves, respectively (**Figure 5**). Spontaneous ICS activity in neonatal SCs has previously been shown to become quiescent at the onset of hearing (23), with suggestion of both spontaneous and evoked ICS waves in adult cochlea (16, 24); the current study extends these prior findings to show clearly that ICS activity can be potentiated by noise exposure. We found that after noise exposure, supporting cells demonstrated increased ICS activity (**Figure 6).** 106 dB noise exposure, sufficient to cause permanent threshold shifts and pro-apoptotic UPR activation, was associated with more prolonged and extensive ICS wave activity in the 24h after noise exposure. In contrast to prior findings of both "fast" and "slow" ICS waves in the adult cochlea (24), we only observed ICS activity comparable to the "fast" waves and similar to the ICS waves found in the neonatal cochlea. It is possible that the current recording configuration and duration was not optimized to detect these longer-duration and slower events.

In addition to the ICS activity in SCs, some hair cells demonstrated an increase in cytosolic Ca^{2+} preceding hair-cell death (**Figure 7**). These transients were reminiscent of those observed in zebrafish hair cells exposed to aminoglycosides (13,14), suggesting a similar role for cytosolic Ca^{2+} accumulation in the events immediately preceding hair-cell death in the noise-exposed mammalian cochlea. Surviving hair cells generally did not demonstrate persistent elevation of cytosolic Ca^{2+}, but instead showed only transient increases. Development of tools to

simultaneously measure cytosolic, ER, and mitochondrial Ca^{2+} in adult cochlear hair cells is necessary to determine how these noise-evoked Ca^{2+} transients relate to prior findings in aminoglycoside-treated zebrafish neuromast hair cells.

These findings — that noise exposure immediately induces ICS waves in supporting cells, Ca^{2+} transients in hair cells, and UPR upregulation across the cochlea, with louder, PTS-associated noise specifically causing persistent ICS waves, UPR shift towards apoptosis, and cytosolic Ca^{2+} increases in hair cells, leading to their death— suggest that Ca^{2+} dysregulation and the UPR may constitute an early mechanism that can control subsequent hair-cell death and PTS. The effectiveness of ISRIB, a small-molecule eIF2B activator that specifically reduces the pro-apoptotic arm of the UPR, in preventing NIHL (6), further supports the notion that the UPR is causally involved in NIHL and can be targeted for treatment. This work demonstrates the need to understand more precisely the timeline and interrelationship of these cellular events and additional molecular mediators that might serve as targets for treatment. In particular, it remains unknown exactly how ICS waves in supporting cells interact with Ca^{2+} transients in hair cells. Indeed, the relationship of ICS waves in astroglia and oligodendrocytes has been extensively studied in the CNS (17-18, 33-34), with myriad associations described between ICS activity and neuronal death, migration, and function, but no universal "code" for how these ICS waves induce specific neuronal fates. The current adult cochlear live-imaging model may represent an opportunity to quantitatively assess the role of SC ICS waves in influencing HC death. Do ICS waves in supporting cells induce hair-cell Ca^{2+} transients and, subsequently, cause hair-cell death? Or do dying hair cells induce ICS waves in the surrounding supporting cells? Indeed, the notion that ICS waves may be triggered by hair-cell damage is supported by studies on ICS waves in neonatal cultures (19,21), where mechanical trauma, laser ablation of hair cells, or neomycin treatment induced ICS waves and ERK1/2 activation in the supporting cells through which the ICS waves propagated. This ERK activation had further downstream

effects on sensory epithelium remodeling and health of surrounding hair cells, illustrating the potential for ICS wave activity to modulate death and survival in the cochlea.

Alternatively, the opposite relationship is possible— ICS waves, which propagate in part through paracrine signaling mediated by ATP released by supporting cells (20), may trigger Ca^{2+} transients in adjacent hair cells. Whereas isolated transients may be tolerated by the hair cells, more intense or persistent ICS activity and ATP release may induce greater ER Ca^{2+} release in hair cells, thereby triggering hair cell death, either through ER Ca^{2+} depletion and the UPR or mitochondrial Ca^{2+} overload and oxidative stress. ATP is elevated in the endolymph after noise exposure (35), and targeting of purinergic receptor signaling has been proposed as a therapeutic strategy for NIHL (36). We found in this study that exogenous ATP induced robust cytosolic Ca^{2+} transients in neonatal hair cells but had no effect on hair cells in the mature-hearing cochlea. This may reflect changes in purinergic receptor expression or intracellular Ca^{2+} homeostasis over the course of hair-cell development (37,38); additionally, Ca^{2+} homeostasis is tightly regulated in hair cells between cytosolic buffering and highly regulated transfer between cytosol, ER, and mitochondria (12), and changes in cytosolic Ca^{2+} alone do not sufficiently predict cytotoxicity relating to downstream ER and mitochondrial effects (14). We observed that OHCs in noise-exposed cochleae did exhibit slow cytosolic Ca^{2+} accumulation that accompanies OHC swelling and fragmentation consistent with OHC death, but we did not independently and concurrently ascertain cell death in this model. Findings in this study are limited the *ex vivo* preparation, in which critical physiologic features such as the endocochlear potential and ionic separation of the cochlear scalae are not maintained. Specific limitations of the current experimental setup - use of a water immersion objective, bath application of drugs - may also cause optical artifacts that limit observation of fast and/or small responses. Development of an acoustically-stimulated, active preparation of the mouse cochlea that provides an endocochlear potential and scalar separation, as has been described for the gerbil cochlea (39) would be valuable for further investigation of the precise interplay between ICS

waves, ATP, subcompartmental Ca^{2+} homeostasis and hair-cell death in the mature, hearing cochlea.

The broad involvement of disorders of Ca^{2+} homeostasis, the UPR, and mitochondrial stress in genetic (12) and acquired (6,7,14) hearing loss highlight the need for further study to understand the underlying mechanisms in physiologically relevant disease models. In this study, we did not comprehensively evaluate all potential pathways by which noise exposure could induce changes in subcellular-compartment Ca^{2+} homeostasis and the associated downstream stress mechanisms. Specifically, we did not assess mitochondrial Ca^{2+} or stress pathways. However, our findings implicating cytosolic Ca^{2+} and the UPR in a consistent model of NIHL in mature-hearing mice does provide strong evidence for their involvement in the pathophysiology of NIHL. Understanding whether ICS waves are directly induced by noise and secondarily cause Ca^{2+} dysregulation in hair cells, or whether ICS waves are a response to hair cell injury that then subsequently helps to determine hair-cell fate, is critical in order to identify targets for treatment.

Conclusion

In conclusion, we found that UPR activation and perturbations in cytosolic Ca^{2+} homeostasis in hair cells and supporting cells are involved in the cochlea's early response to acoustic overstimulation. Given the critical role of the UPR, ICS waves, and cellular Ca^{2+} homeostasis in stress responses and subsequent cell fate, these findings suggest that targeting these pathways could be successful in treating NIHL. Further investigation into the specific mechanisms linking hair-cell and supporting-cell Ca^{2+} homeostasis and the UPR are necessary to more precisely identify targets for treatment.

Methods

Sex as a biological variable

Our study examined male and female animals, and similar findings are reported for both sexes.

Mouse models and cochlear preparation

Sox2Cre (Jackson Laboratory #008454) or Myo15Cre (15) mice were bred with Ai95D mice (Jackson Laboratory #028865) for expression of GCaMP in supporting or hair cells, respectively. For wild-type noise exposures, 7-8-week-old CBA/CaJ mice (Jackson Laboratory, #000654) were used. Postnatal day 3-5 (P3-5) neonatal cochlear explant cultures were established as described (6). Briefly, P3-5 mice were decapitated, temporal bones extracted, cochlear ducts removed and plated on glass cover slips coated in Cell-Tak (Corning, 354240) with the apical surface of the epithelium facing up. Tectorial membrane was left intact and cochleae cultured overnight in DMEM supplemented with 10% FBS at 37°C in 5% CO_2. Cultures that were grossly intact and remained fully adherent to the coverslip without sign of contamination were used for live imaging after overnight culture.

For live imaging in juvenile, mature-hearing cochleae, explant preparation was adapted from prior studies (24, 26, 31, 40), 7-8-week old mice were euthanized with carbon dioxide and decapitated immediately after noise exposure. The temporal bone was extracted from the skull by removal of the auditory bulla and then placed in ice-cold HBSS. Soft tissue and ossicles were removed with fine forceps and the otic capsule mounted on a custom 3D printed slide fixated in a hole on a plastic coverslip. Fresh HBSS was applied and the bone covering the apical turn of the cochlea was removed, preserving the membranous labyrinth and exposing the helicotrema. Reissner's membrane was removed and the preparation used immediately for imaging. Time from euthanasia to imaging averaged less than 10 min. In all cases, only one cochlea was used per animal for live imaging.

Resonance (for Sox2Cre-GCaMP neonate) or line-scanning (for all other models) confocal imaging was performed on an upright Nikon A1R confocal microscope using a 60x water-immersion objective (NIR Apo, 1.0 NA), with temperature and CO_2 control using a stagetop incubator (OKOlab). Optical sections in the x-y plane were recorded at 1x averaging, 1.2 AU pinhole, 1.1 dwell time, displaying the entire inner sulcus (IS), outer sulcus (OS) and hair cell regions in the middle cochlear turn (neonates) and apical cochlear turn (8-10 kHz region, juveniles).

For neonatal cultures, baseline imaging was performed for 3 minutes, followed by vehicle (media), thapsigargin (Tocris) and/or sodium orthovanadate (Calbiochem) application at t = 3 min and, for Myo15Cre-GCaMP only, 1 mM ATP (Sigma) at t = 5 min. All drugs were bath-applied to the final indicated concentrations and not washed out. A total of 20 min imaging was performed, with interval between each successive image of 1 s for Sox2Cre-GCaMP and 2 s for Myo15Cre-GCaMP. For imaging of juvenile, mature-hearing, a single 10-min continuous imaging session was performed, with an interval of 2 s.

UPR marker gene quantification

UPR marker gene expression was quantified in cochleae from noise-exposed animals as described (6). Briefly, at the indicated times after completion of noise exposure, animals were euthanized and cochleae harvested onto dry ice. Both cochleae from a single animal were pooled into a single specimen. Cochlear RNA was isolated from mice exposed to noise, or unexposed, using TRIzol Reagent (Thermo Fisher Scientific, 15596026). RNA quality was determined using a spectrophotometer and was reverse transcribed using Superscript IV VILO master mix (Thermo Fisher Scientific, 11756050). Expression levels of three UPR markers (*BiP*, indicative of UPR activation; *Chop*, correlated with pro-apoptotic activity of the UPR; and *S-Xbp1*, associated with pro-homeostatic activity of the UPR) as well as *Gapdh* (as reference)

were measured by qPCR and quantified against *Gapdh* and unexposed controls using the $2^{-\Delta\Delta CT}$ method (**Supplemental Figure S6**). Samples with inadequate *Gapdh* levels (defined as CT>24) were excluded from analysis. The ratio of *Chop* over *S-Xbp1* was used as a marker of the pro-apoptotic state of the UPR (15).

In a separate experiment, mRNA was isolated identically from noise exposed and unexposed mouse cochlea, and cDNA was tested was using a real-time RT^2 Profiler PCR Array (UPR Panel, QIAGEN PAMM-089Z) in combination with RT^2 SYBR Green qPCR Mastermix (QIAGEN, 330529). The PCR reaction was run on a Bio-Rad CFX 384 real-time PCR cycler. C_T values were exported and data analysis conducted using the GeneGlobe Data Analysis Center (QIAGEN). Fold change/regulation was calculated using the $2^{-\Delta\Delta CT}$ method. Student's t test was used to compare $2^{-\Delta CT}$ values for each gene in control vs noise exposure conditions.

Image processing

Ca^{2+} fluorescence measurements were performed on regions of interest (ROIs) slightly larger than a cell, as done previously (6). Briefly, images were reoriented such that the hair cells were parallel to the bottom of the image. 325 ROIs, each 56 x 56 pixels (11 μm x 11 μm) in area were defined (ImageJ), and mean fluorescence intensity measured for every ROI at each timepoint. Ca^{2+} peak activity from each ROI-specific fluorescence timecourse was captured using a custom in-house script (Matlab, R2023a). Threshold for detection of a Ca^{2+} peak was set at 10 times the standard deviation of the baseline fluorescence measurement.

Noise exposure and auditory testing

For NIHL induction, mice were exposed to 94, 98, or 106 dB SPL 8-16 kHz octave-band noise in a custom-built reverberant chamber as described (6), which respectively cause no hearing loss (94 dB), TTS with cochlear synaptopathy (98 dB) (16), and PTS with hair-cell death (106 dB) (6). Hearing was tested in mice by measuring auditory brainstem response (ABR) thresholds in response to broadband tone pips at 8, 16, and 32 kHz in the sound field using a standard commercial system (RZ6, Tucker-Davis Technologies) in a soundproof chamber as described (6).

Experimental rigor and statistical analysis

Prior to analysis, data distribution was assessed for normality with the Shapiro-Wilks test. For normally-distributed data, outliers were removed (ROUT method, Q=1%). For comparison between treatment groups, we used Student's t-test (for normally-distributed data) or Mann-Whitney rank-sum test (for non-normally-distributed data) for comparisons between 2 groups, or one-way ANOVA, followed by post-hoc Dunnett's multiple comparison tests, for comparisons between >2 groups. Unless otherwise mentioned, results are presented as means +/- sem with sample sizes and p values between designated comparison groups as indicated in the figure legends, with a p-value <0.05 as significant, and lower p values indicated for specific comparisons. Statistical analyses were performed with GraphPad Prism 9.5.1. Sex was evaluated as a biological variable. UPR gene expression (**Figure 1**) and ABR thresholds (**Figure S1**) after different noise exposure levels were tested for male and female mice, and no significant differences found (unpaired two-tailed t-test with adjustment for multiple comparisons (Bonferroni correction for 3 simultaneous comparisons, for 3 noise-exposure levels). Because no differences were seen in these core measures between sexes, all subsequent analyses used pooled male and female mice.

Study approval

This study was approved by the Institutional Animal Care and Use Committee of the University of California, San Francisco (AN1999783-00).

Data Availability

All underlying data and supporting analytic code used in this study are either present in the published manuscript or the accompanying Supporting Data Values supplement, or will be shared upon reasonable request made by e-mail to the corresponding author (DKC).

Author Contributions

Initial design: YP, JL, EHS, DKC. Experimental and ethical oversight, and funding: EHS and DKC. Experimental contributions: YP, JL, NIM, IRM, PS, and DKC. Data and statistical analysis: YP, JL, NIM, IRM, PS, and DKC. Manuscript drafting: YP, JL, and DKC. Manuscript review and approval: all authors. Multiple first and corresponding authors: YP and JL share first position, and EHS and DKC share final position. This work was a collaboration between groups focused on cell biology and genetics (conducted by JL and EHS) and auditory physiology and imaging (conducted by YP, NIM, IRM, PS and DKC). Because the physiology work constituted >50% of the actual content in the study, YP is listed first among the shared first position, and DKC is listed last among the shared final position.

Acknowledgements

This study was funded by NIDCD R01 DC018583 (to DKC and EHS); and “Generation of cell lines to understand TMTC4, a novel human deafness gene,” from Hearing Research, Inc. (to DKC).

Figures

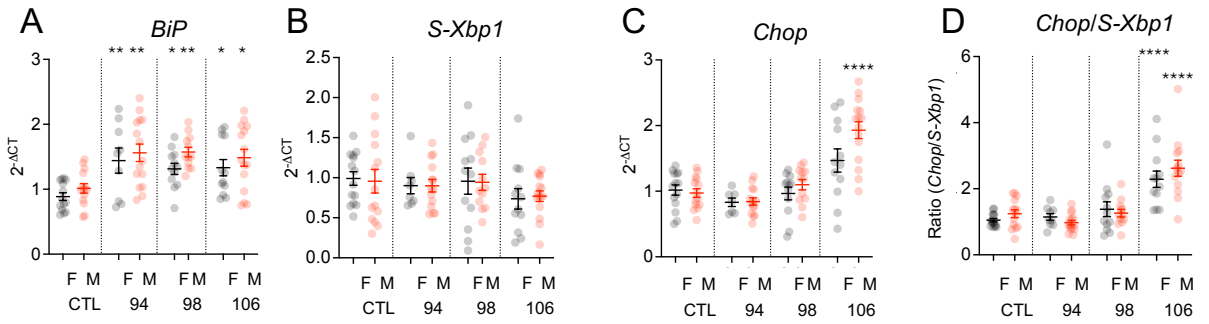

Figure 1. Noise exposure induces UPR upregulation in the cochlea *in vivo*. To investigate the sound level dose-dependence of UPR activation after acoustic overstimulation, we exposed 8-week-old male and female wild-type CBA/J mice to 8-16 kHz octave-band noise for 2 hours at 94, 98 106, levels that respectively induce no hearing loss, temporary threshold shift (TTS) with cochlear synaptopathy, and permanent threshold shift (PTS) with hair-cell death, respectively. The two cochleae from each animal were harvested and pooled for qPCR measurement of *BiP* (A), *S-Xbp1* (B), *Chop* (C) and ratio of *Chop/S-Xbp1* (D) mRNA expression using the $2^{-\Delta CT}$ method relative to *Gapdh* expression and normalized to control (non-noise-exposed) levels. Data were cleaned by removing outliers (ROUT method, Q=1%; 6/412 (1.5%) datapoints removed) and compared with one-way ANOVA with Dunnett's test for multiple comparisons against control for each condition. Data are presented as means ± SEM, with individual animals shown as dots. * $p < 0.05$; ** $p < 0.01$; *** $p < 0.001$; **** $p < 0.0001$. N = 14 mice (CTL-F); 14 (CTL-M); 9 (94 dB – F); 15 (94 dB – M); 12 (98 dB – F); 12 (98 dB – M); 12 (106 dB – F); 15 (106 dB – M).

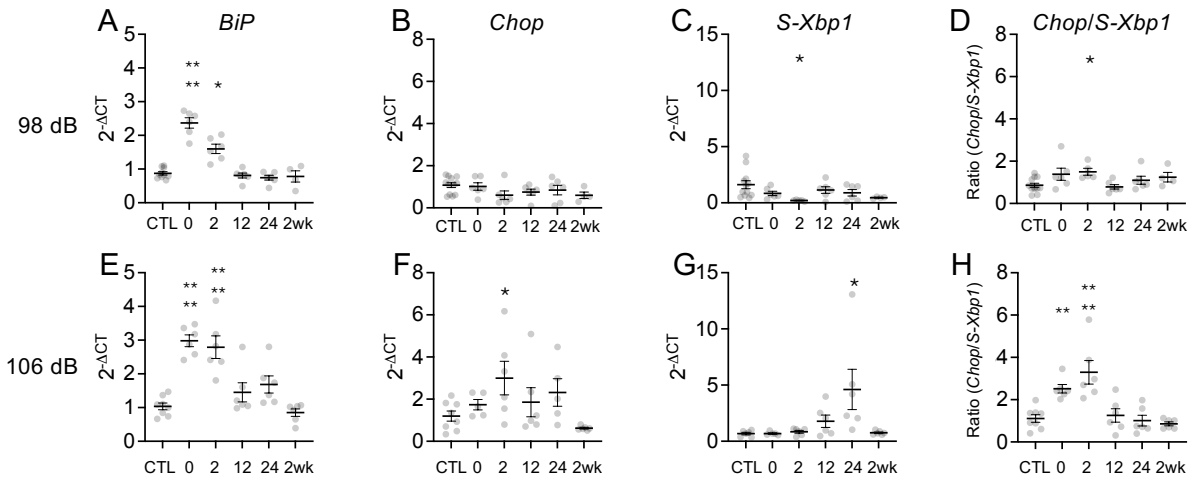

Figure 2. Noise exposure induces rapid UPR upregulation in the cochlea *in vivo.* To investigate the temporal evolution of the UPR after acoustic overstimulation, we exposed 8-week-old male wild-type CBA/J mice to 8-16 kHz octave-band noise for 2 hours at 98 dB SPL (A-D), which induces TTS, or 106 dB SPL (E-H), which induces PTS. The two cochleae from each animal were harvested and pooled at the indicated timepoints after noise exposure for qPCR measurement of *BiP*, *S-Xbp1*, and *Chop* mRNA expression using the $2^{-\Delta CT}$ method relative to *Gapdh* expression and normalized against control (non-noise-exposed) levels. Data were cleaned by removing outliers (ROUT method, Q=1%; 9/312 (2.9%) datapoints removed) and compared with one-way ANOVA with Dunnett's test for multiple comparisons against control for each condition. Data are presented as means ± SEM, with individual animals shown as dots. * $p < 0.05$; ** $p < 0.01$; *** $p < 0.001$; **** $p < 0.0001$. N = 12 mice (CTL – 98 dB); 8 (CTL – 106 dB); 6 (0, 2, 12, 24h, 98 dB and 106 dB); 6 (2wk – 106 dB); 4 (2wk – 98 dB).

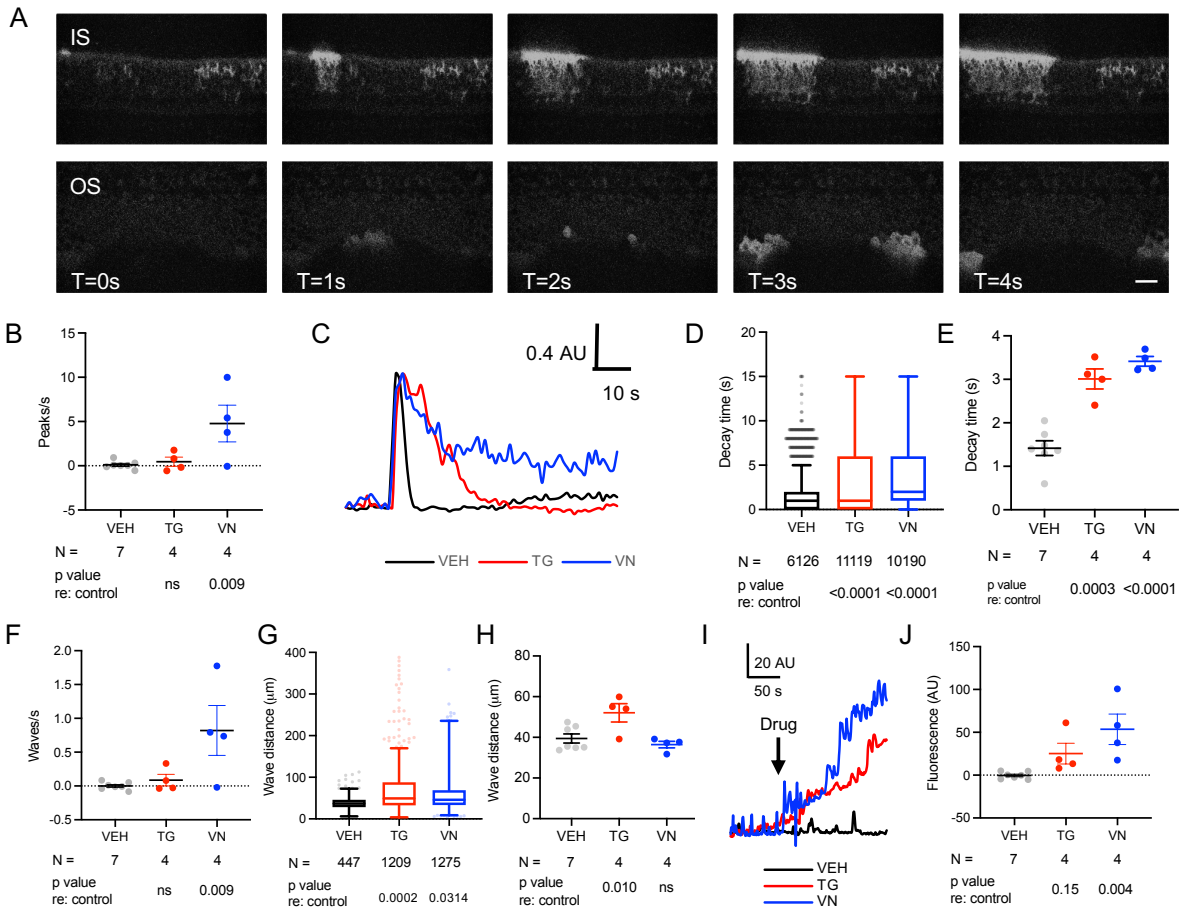

Figure 3. Ca^{2+} activity in neonatal cochlear supporting cells. A. Live imaging of Sox2Cre-GCaMP neonatal cochlea. In supporting cells of the inner sulcus (IS) and outer sulcus (OS) of the neonatal cochlea, spontaneous intercellular Ca^{2+} waves are observed. Time interval between successive images is 1s. Scale bar: 20 μm. Representative video also shown in **Supplemental Video 1**. **B. Change in number of Ca^{2+} peaks per second after drug treatment.** Compared to baseline (media only), no change in frequency of Ca^{2+} peaks is seen with vehicle (VEH, black) or 1 μM thapsigargin (TG, red); 5 μM vanadate (VN, blue) induced increased Ca^{2+} peak activity. **C-E. Ca^{2+} decay time with drug treatment.** Fluorescence levels **(C)** and peak decay time at the individual peak **(D)** or cochlea **(E)** level demonstrate significant prolongation of return to baseline Ca^{2+} levels in the presence of TG or VN. In **(C),** peak height is normalized to maximum amplitude for each peak. **F. Change in number of ICS waves per**

second after drug treatment. No change in frequency of ICS waves is seen with vehicle (VEH) or thapsigargin (TG); vanadate (VN) induced more ICS activity. **F-G. ICS wave distance propagation with drug treatment.** ICS waves travelled significantly farther in the presence of TG, but not VN, when compared at the individual wave **(F)** or cochlea **(G)** level. **I-J. Change in steady-state Ca^{2+} after drug treatment.** Fluorescence levels **(I)** and mean amplitude **(J)** over a 300s recording period, representing steady-state Ca^{2+} level across the entire cochlea, increased after TG and VN, but not VEH application. **B, E, F, H, J:** Means ± SEM, with individual cochlea-level values as dots. Groups were compared with one-way ANOVA with Dunnett's test for multiple comparisons against control for each condition, with p values as indicated. Sample sizes tested enabled detection of effect size > 1.98x SD with 80% power. **D and G:** Tukey plots (box: 1st quartile/median/3rd quartile; whiskers: 10th and 90th percentile; dots: individual points outside the whiskers) representing all peaks **(D)** or waves **(G)** measured under the indicated conditions. P values are as indicated for pairwise comparisons versus control (VEH) on 2-tailed unpaired Student's t test. ns, not significant. AU, arbitrary units.

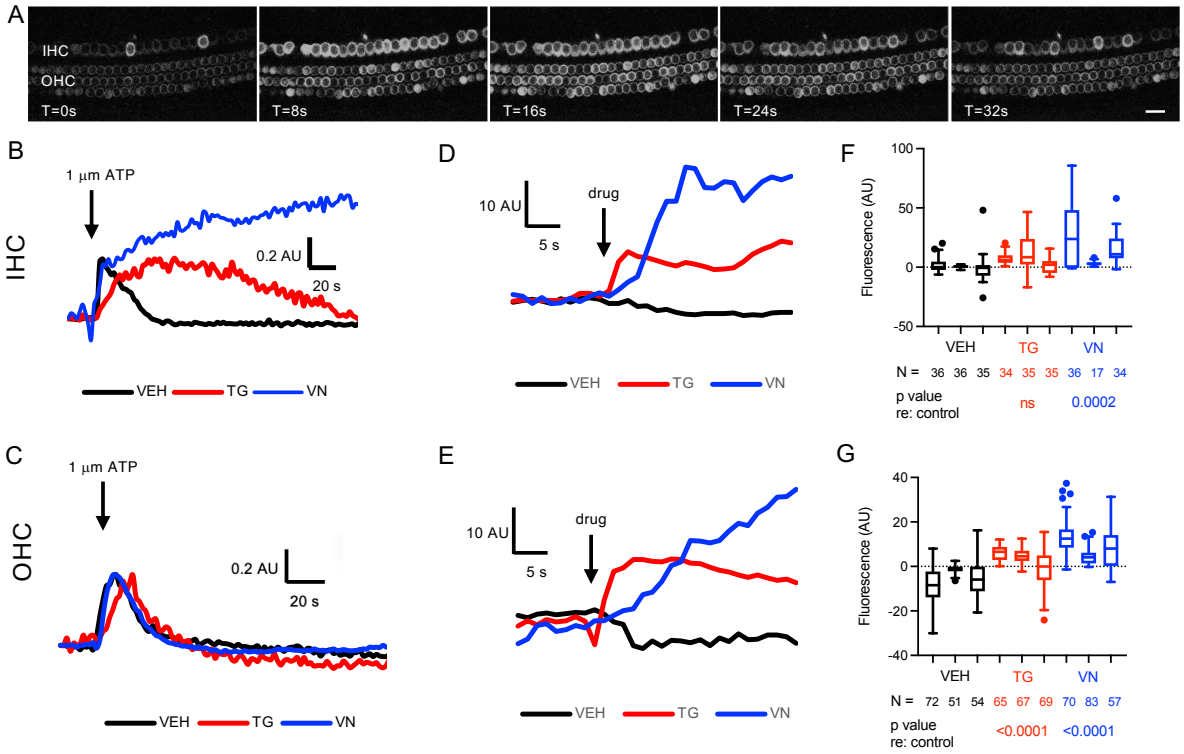

Figure 4. Ca^{2+} activity in neonatal cochlear hair cells. A. Live imaging of in Myo15Cre-GCaMP neonatal cochlea. No spontaneous Ca^{2+} activity is seen in hair cells of the neonatal cochlea. However, application of 1 μm ATP (applied after the leftmost panel) induced an increase in cytosolic Ca^{2+} with subsequent return to baseline in both inner hair cells (IHCs) and outer hair cells (OHCs). Time interval between successive images is 8s. Scale bar: 20 μm. Representative video also shown in **Supplemental Video 2**. **B-C. ATP-induced Ca^{2+} peaks.** In an individual cochlear IHC **(B)**, bath application of 1 μm ATP (arrow) induced an increase in Ca^{2+} in the presence of vehicle (VEH, black), thapsigargin (TG, red), and vanadate (VN, blue), with prolonged onset and decay time with TG and prolonged elevation with no return to baseline in the presence of VN. An OHC **(C)** was also responsive to ATP; however, TG and VN had minimal effect on return to baseline. For both **(B)** and **(C)**, peak height is normalized to

maximum amplitude of the initial ATP-induced peak. **D-G. Change in Ca^{2+} after drug treatment.** Treatment with TG (red) and VN (blue) induced initial increases in Ca^{2+}, as seen in mean fluorescence tracings across IHC **(D)** and OHC regions **(E)** immediately after drug treatment (arrow). Comparison of steady-state Ca^{2+} levels after drug treatment **(F)** and **(G)** showed that TG induced a significant persistent increase in Ca^{2+} in OHCs, **(G)**, but not IHCs **(F)**, where VN increased steady-state Ca^{2+} in both IHCs and OHCs**. F-G.** Tukey plots (box: 1st quartile/median/3rd quartile; whiskers: 10th and 90th percentile; dots: individual points outside the whiskers) representing all cells measured in individual cochleae under the indicated conditions. Groups were compared with two-way ANOVA to detect treatment or cochlea-specific differences in fluorescence; p values indicate treatment effect for the indicated drug compared to control. Sample sizes tested enabled detection of effect size > 3.07x SD with 80% power. ns, not significant. AU, arbitrary units.

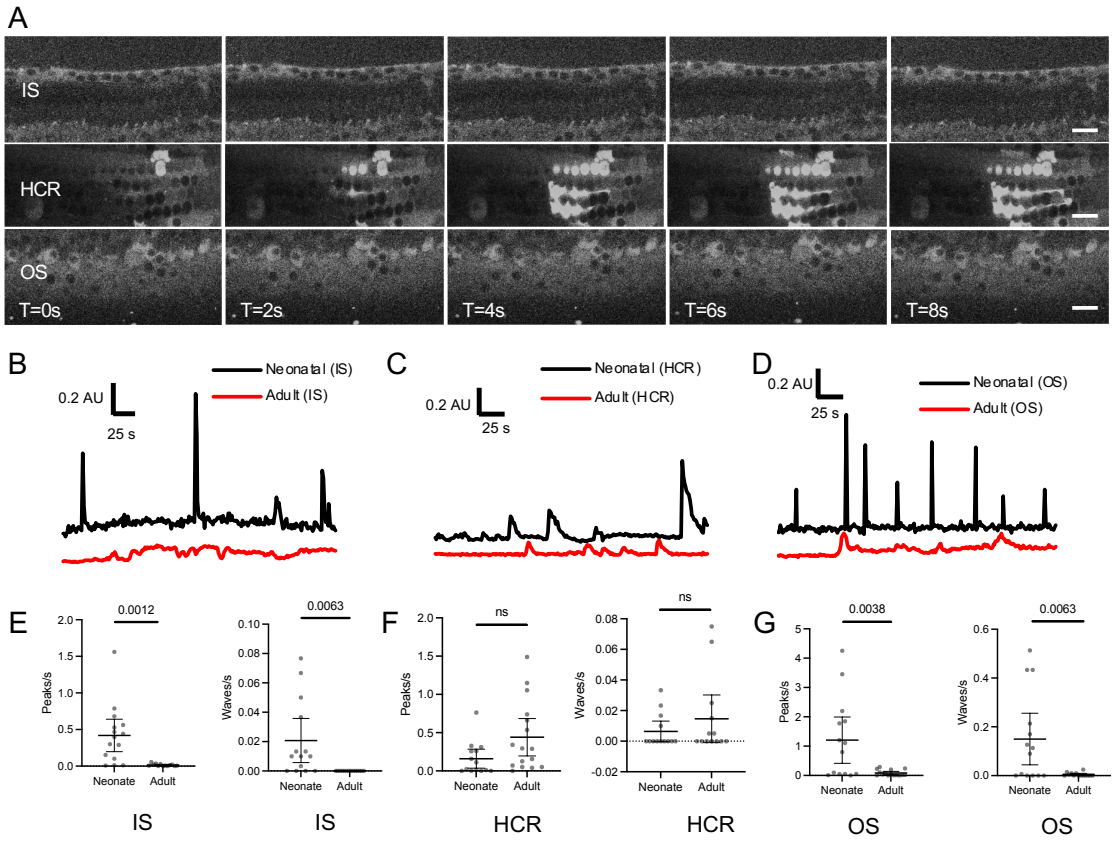

Figure 5. Ca^{2+} activity in adult cochlear supporting cells. A. Live imaging of Sox2Cre-GCaMP adult cochlea. Spontaneous Ca^{2+} activity was evaluated in supporting cells of the adult cochlea within the inner sulcus (IS), hair-cell region (HCR), and outer sulcus (OS). Time interval between successive images is 2s. Scale bar: 20 μm. Representative video shown in **Supplemental Video 4**. **B-G. Activity in neonatal vs adult cochlea.** Compared with neonatal cochlea (black), single cells in the IS (**B**) and OS (**D**) of the adult cochlea (red) showed reduced spontaneous Ca^{2+} peak activity. A supporting cell in the adult HCR (**C**) showed comparable spontaneous activity to neonatal cochlea. Number of peaks and waves per second was significantly higher in neonatal versus adult cochlea in both IS **(E)** and OS **(G)** regions, and not significantly different in the HCR. **E-G.** Means ± SEM with individual values in gray. P values

as indicated (black bars) on pairwise comparison between neonatal and adult cochlea using 2-tailed, unpaired Student's t test. N = 15 (neonate) and 16 (adult) cochleae. AU, arbitrary units.

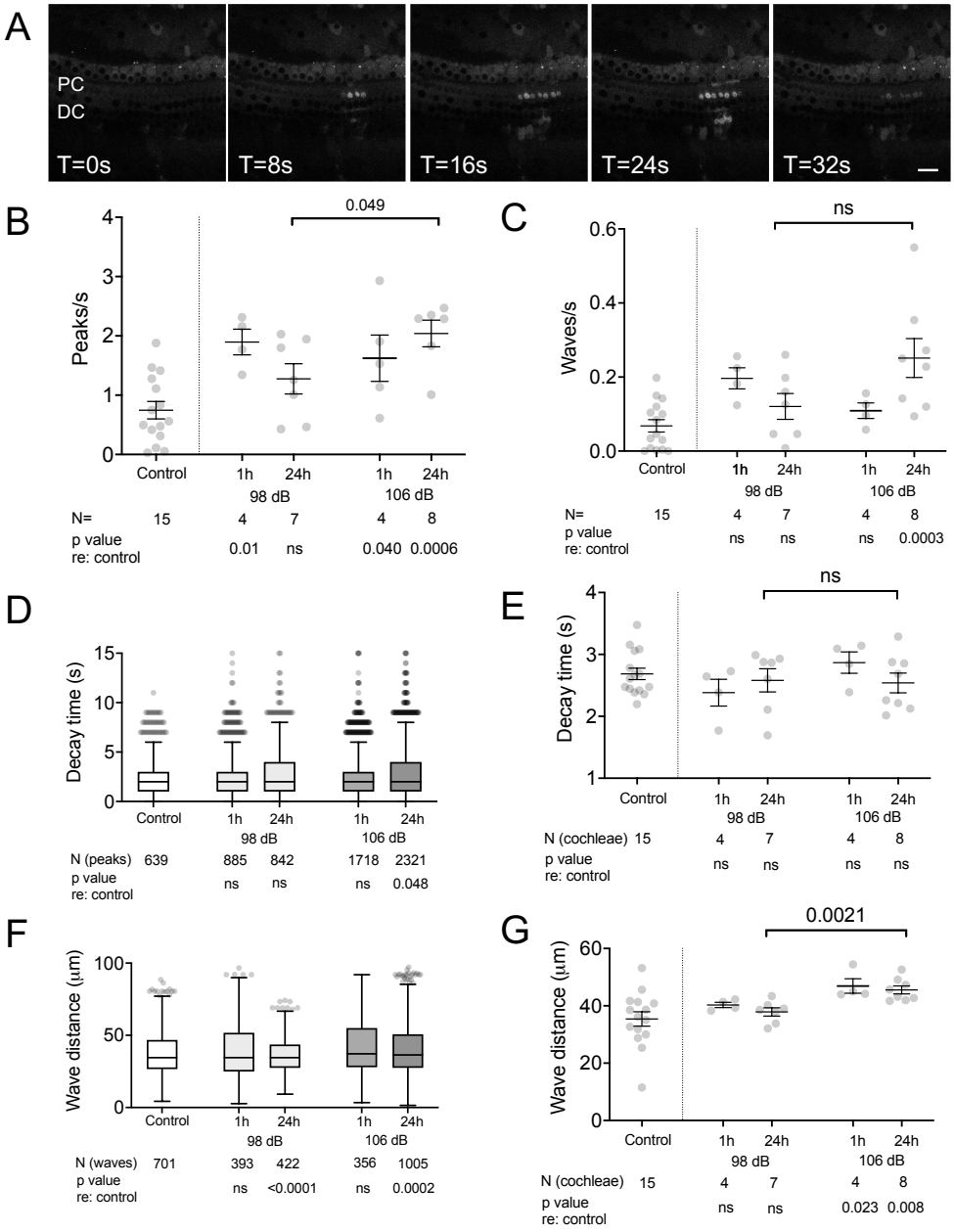

Figure 6. Ca^{2+} activity in adult cochlear supporting cells. A. Live imaging of noise-exposed Sox2Cre-GCaMP adult cochlea. Pre-exposure to 98-dB SPL noise induces ICS wave activity in supporting cells of the adult cochlea, including pillar cells (PC) and Dieter's cells

(DC). Time interval between successive images is 8s. Scale bar: 20 μm. Representative video also shown in **Supplemental Video 5**. **B-C. Effect of noise exposure on Ca^{2+} peak and ICS wave activity.** Compared with control, non-noise-exposed cochleae, cochleae from mice exposed to 98 dB as well as 106 dB noise showed increased number of Ca^{2+} peaks **(B)** and ICS waves **(C)** 1h after beginning of noise exposure. 24h after completion of noise exposure, 98-dB-exposed mice had no significant increase in either Ca^{2+} peaks or ICS waves compared to control, whereas 106-dB-exposed mice had persistent elevation in both Ca^{2+} peak activity and ICS waves. **D-E. Effect of noise exposure on Ca^{2+} peak decay time.** Ca^{2+} peak decay time is compared under the indicated conditions at the individual peak **(D)** or cochlea **(E)** level. **F-G. Effect of noise exposure on ICS wave propagation distance.** Distance traveled for ICS waves, compared at the individual wave **(F)** and cochlea **(G)** level was increased after 106-dB, but not 98-dB noise exposure. **B-C, E, G.** Means ± sem, with individual values in gray. Sample size refers to the number of individual cochleae**. D, F.** Tukey plots (box: 1st quartile/median/3rd quartile; whiskers: 10th and 90th percentile; dots: individual points outside the whiskers) are shown. Sample size refers to the number of individual cochleae (**B-C, E, G**) peaks **(D),** or waves **(F)** analyzed. Groups were compared with one-way ANOVA with Dunnett's test for multiple comparisons against control for each condition, with p values as indicated underneath each graph. Additionally, 2-tailed unpaired Student's t test was performed to compare values at the 24h timepoint after noise exposure, as indicated in brackets with associated p values. ns, not significant.

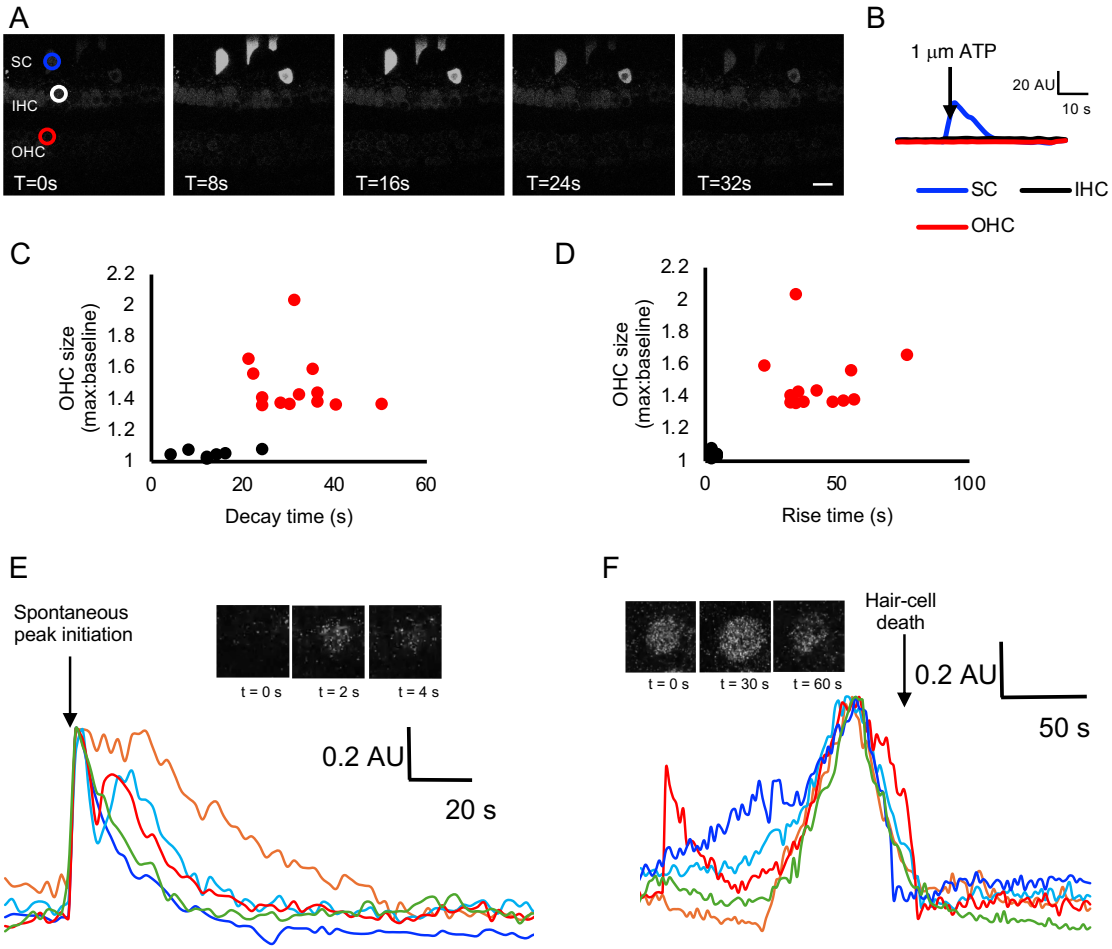

Figure 7. Live imaging of Myo15Cre-GCaMP adult cochlea. A-B. In the adult cochlea, no spontaneous Ca^{2+} peak activity is seen in hair cells **(A)**. Though an inner-sulcus supporting cell (SC, blue) with off-target expression of GCaMP responded to ATP (applied after the leftmost image) with a Ca^{2+} peak, neither an inner hair cell (IHC, white/black) nor an outer hair cell (OHC, red) was responsive. Time interval between successive images is 8s. Scale bar: 20 μm. Representative video also shown in **Supplemental Video 6**. **C-F. Noise-induced Ca^{2+}**

transients. In fluorescence traces from OHCs from cochleae exposed to 106-dB noise, cytosolic Ca^{2+} transients were observed. Rise time (time from baseline to half-maximum, in s) **(C)** and decay time **(D)** for 20 Ca^{2+} transients was plotted against OHC maximum size relative to baseline, demonstrating two populations of transients— "slow" transients (red) that were associated with OHC swelling and fragmentation, and "fast" transients (black) that were not. Individual traces of fast **(E)** and slow **(F)** OHC transients are shown, with insets depicting still images of these events corresponding to video shown in **Supplemental Video 6**. Traces are normalized to maximal peak amplitude and aligned at the time of spontaneous peak initiation **(E)** or the time of hair-cell fragmentation **(F).** AU, arbitrary units.

References

1. Carroll YI, Eichwald J, Scinicariello F et al. Vital Signs: Noise-Induced Hearing Loss Among Adults in the United States 2011-2012. *MMWR Morb Mortal Wkly Rep.* 2017; 66:139-144.
2. Yamane H, Nakai Y, Takayama M, Iguchi H, Nakagawa T, Kojima A. Appearance of free radicals in the guinea pig inner ear after noise-induced acoustic trauma. *Eur Arch Otorhinolaryngol.* 1995; 252:504-508.
3. Kurabi A, Keithley EM, Housley GD, Ryan AF, Wong AC. Cellular mechanisms of noise-induced hearing loss. *Hear Res.* 2017; 349:129-137.
4. Maeda Y, Fukushima K, Omichi R, Kariya S, Nishizaki K. Time courses of changes in phospho-and total-MAP kinases in the cochlea after intense noise exposure. *PloS One.* 2013; 8(3):e58775.
5. Li P, Li S, Wang L, Li H, Wang Y, Liu H, Wang X, Zhu X, Liu Z, Ye F, Zhang Y. Mitochondrial dysfunction in hearing loss: Oxidative stress, autophagy and NLRP3 inflammasome. *Front Cell Dev Biol.* 2023; 11:1119773.
6. Li J, Akil O, Rouse SL, McLaughlin CW, Matthews IR, Chan DK, and Sherr EH. Deletion of Tmtc4 activates the unfolded protein response and causes postnatal hearing loss. *J Clin Invest.* 2018; 128(11):5150-5162.
7. Wang X, Zhu Y, Long H, Pan S, Xiong H, Fang Q, Hill K, Lai R, Yuan H, Sha SH. Mitochondrial Calcium Transporters Mediate Sensitivity to Noise-Induced Losses of Hair Cells and Cochlear Synapses. *Front Mol Neurosci.* 2019; 11:469.
8. Wang J, Van De Water TR, Bonny C, de Ribaupierre F, Puel JL, Zine A. A peptide inhibitor of c-Jun N-terminal kinase protects against both aminoglycoside and acoustic trauma-induced auditory hair cell death and hearing loss. *J Neurosci.* 2003; 23(24):8596-607.
9. Kopke R, Slade MD, Jackson R, Hammill T, Fausti S, Lonsbury-Martin B, Sanderson A, Dreisbach L, Rabinowitz P, Torre P 3rd, Balough B. Efficacy and safety of N-acetylcysteine in prevention of noise induced hearing loss: a randomized clinical trial. *Hear Res.* 2015; 323:40-50.

10. Eshraghi AA, Aranke M, Salvi R, Ding D, Coleman JKM Jr, Ocak E, Mittal R, Meyer T. Preclinical and clinical otoprotective applications of cell-penetrating peptide D-JNKI-1 (AM-111). *Hear Res.* 2018; 368:86-91.
11. Chang PH, Liu CW, Hung SH, Kang YN. Effect of N-acetyl-cysteine in prevention of noise-induced hearing loss: a systematic review and meta-analysis of randomized controlled trials. *Arch Med Sci.* 2021; 18(6):1535-1541.
12. Richard EM, Maurice T, Delprat B. Calcium signaling and genetic rare diseases: An auditory perspective. *Cell Calcium.* 2023; 110:102702.
13. Esterberg R, Hailey DW, Coffin AB, Raible DW, and Rubel EW. Disruption of intracellular calcium regulation is integral to aminoglycoside-induced hair cell death. *J Neurosci.* 2013; 33(17): 7513-25.
14. Esterberg R, Hailey DW, Rubel EW, Raible DW. ER-mitochondrial calcium flow underlies vulnerability of mechanosensory hair cells to damage. *J Neurosci.* 2014; 34(29):9703-19.
15. Li J, Choi BY, Eltawil Y, Ismail Mohamad N, Park Y, Matthews IR, Han JH, Kim BJ, Sherr EH, Chan DK. TMTC4 is a hair cell-specific human deafness gene. *JCI Insight.* 2023; 8(24):e172665
16. Rouse SL, Matthews IR, Li J, Sherr EH, Chan DK. Integrated stress response inhibition provides sex-dependent protection against noise-induced cochlear synaptopathy. *Sci Rep.* 2020; 10(1):18063.
17. Scemes E, Giaume C. Astrocyte calcium waves: what they are and what they do. *Glia.* 2006; 54(7):716-725.
18. Leybaert L, Sanderson MJ. Intercellular Ca(2+) waves: mechanisms and function. *Physiol Rev.* 2012; 92(3):1359-92.
19. Gale JE, Piazza V, Ciobotaru CD, Mammano F. A mechanism for sensing noise damage in the inner ear. *Curr Biol.* 2004; 14(6):526-9.
20. Majumder P, Crispino G, Rodriguez L, Ciubotaru CD, Anselmi F, Piazza V, Bortolozzi M, Mammano F. ATP-mediated cell-cell signaling in the organ of Corti: the role of connexin channels. *Purinergic Signal.* 2010; 6(2):167-87.

21. Lahne M and Gale JE. Damage-induced activation of ERK1/2 in cochlear supporting cells is a hair cell death-promoting signal that depends on extracellular ATP and calcium. *J Neurosci.* 2008; 28(19):4918-28.
22. Tritsch NX, Yi E, Gale JE, Glowatzki E, Bergles DE. The origin of spontaneous activity in the developing auditory system. *Nature.* 2007; 450(7166):50-5.
23. Tritsch NX and Bergles DE. Developmental regulation of spontaneous activity in the mammalian cochlea. *J Neurosci.* 2010; 30(4):1539-1550.
24. Sirko P, Gale JE, Ashmore JF. Intercellular Ca^{2+} signalling in the adult mouse cochlea. *J Physiol.* 2019. 597(1):303-317.
25. Piazza V, Ciubotaru CD, Gale JE, Mammano F. Purinergic signalling and intercellular Ca^{2+} wave propagation in the organ of Corti. *Cell Calcium.* 2007; 41(1):77-86.
26. Chan DK, Rouse SL. Sound-Induced Intracellular Ca^{2+} Dynamics in the Adult Hearing Cochlea. *PLoS One.* 2016; 11(12):e0167850.
27. Walter and Ron D. The unfolded protein response: from stress pathway to homeostatic regulation. *Science.* 2011; 334(6059):1081-6.
28. Lu M, Lawrence DA, Marsters S *et al.* Opposing unfolded-protein-response signals converge on death receptor 5 to control apoptosis. *Science*. 2014; 345:98–101.
29. Jongkamonwiwat N et al. Noise Exposures Causing Hearing Loss Generate Proteotoxic Stress and Activate the Proteostasis Network. *Cell Rep.* 2020; 33(8):108431.
30. Milon B et al. A cell-type-specific atlas of the inner ear transcriptional response to acoustic trauma. *Cell Rep.* 2021; 36(13):109758.
31. Ismail Mohamad N, Santra P, Park Y, Matthews IR, Taketa E, Chan DK. Synaptic ribbon dynamics after noise exposure in the hearing cochlea. *Commun Biol*. 2024; 7(1):421.
32. Müller M, von Hünerbein K, Hoidis S, Smolders JW. A physiological place-frequency map of the cochlea in the CBA/J mouse. *Hear Res.* 2005; 202(1-2):63-73.
33. Lim D, Semyanov A, Genazzani A, Verkhratsky A. Calcium signaling in neuroglia. *Int Rev Cell Mol Biol.* 2021; 362:1-53.

34. Paudel S, Yue M, Nalamalapu R, Saha MS. Deciphering the Calcium Code: A Review of Calcium Activity Analysis Methods Employed to Identify Meaningful Activity in Early Neural Development. *Biomolecules.* 2024; 14(1):138.
35. Muñoz DJ, Kendrick IS, Rassam M, Thorne PR. Vesicular storage of adenosine triphosphate in the guinea-pig cochlear lateral wall and concentrations of ATP in the endolymph during sound exposure and hypoxia. *Acta Otolaryngol.* 2001; 121(1):10-5.
36. Berekméri E, Szepesy J, Köles L, Zelles T. Purinergic signaling in the organ of Corti: Potential therapeutic targets of sensorineural hearing losses. *Brain Res Bull.* 2019; 151:109-118.
37. Jovanovic S, Milenkovic I. Purinergic Modulation of Activity in the Developing Auditory Pathway. *Neurosci Bull.* 2020; 36(11):1285-1298.
38. Babola TA, Li S, Wang Z, Kersbergen CJ, Elgoyhen AB, Coate TM, Bergles DE. Purinergic Signaling Controls Spontaneous Activity in the Auditory System throughout Early Development. *J Neurosci.* 2021; 41(4):594-612.
39. Chan DK, Hudspeth AJ. Ca^{2+} current-driven nonlinear amplification by the mammalian cochlea in vitro. *Nat Neurosci.* 2005; 8(2):149-55.
40. Majumder P, Duchen MR, Gale JE. Cellular glutathione content in the organ of Corti and its role during ototoxicity. *Front Cell Neurosci*. 2015; 9:143.